IEEE Access
Multidisciplinary : Rapid Review : Open Access Journal

Received July 7, 2021, accepted July 11, 2021, date of publication July 26, 2021, date of current version August 5, 2021.

Digital Object Identifier 10.1109/ACCESS.2021.3099863

Implementation and Evaluation of a 3.3 kWp IoT-Based Photovoltaic Microgrid-Interactive Configuration

WALUYO, (Member, IEEE), ANDRE WIDURA, FEBRIAN HADIATNA, (Member, IEEE), AND RANGGA MAULANA

Department of Electrical Engineering, Institut Teknologi Nasional Bandung (Itenas), Bandung 40124, Indonesia

Corresponding author: Waluyo (waluyo@itenas.ac.id)

This work was supported in part by Directorate of Research and Community Service, Directorate General of Research Strengthening and Development, Ministry of Research, Technology and Higher Education, Indonesia, under Grant 285/B.05/LPPM-Itenas/III/2019.

ABSTRACT Recently, PV grid integrated power generation has been intensively promoted, involving monitoring systems and inverters. Thus, two important issues are monitoring parameters and inverter efficiency. Therefore, this research used an IoT-based monitoring and recording system for the implementation and evaluation of a 3.3 kWp PV microgrid-interactive configuration integrated into a nominal 220-volt network. This network comprises a hybrid inverter, protection modules, an IoT-based monitoring facility, and four batteries. New ideas include more monitoring parameters, including statistical analyses and sorting power flow-based inverter efficiencies, as well as additional solar module scenarios for economic analysis. The results showed that the estimated generated and actual generated energies within 40 days were 596.60 kWh and 550.00 kWh, respectively. The total load consumed, grid exported and imported energies, battery charge, and discharge energies were 263.30 kWh, 278.30 kWh, 7.70 kWh, 45.20 kWh, and 38.70 kWh, respectively. The CF, PR, and system efficiency were 17.36%, 84.8%, and 12.73%, respectively, in the performance analysis. The typical inverter efficiencies were 98.03%, 98.03%, 93.81%, 98.01%, 98.05%, and 91.67% for the six power flow categories. According to the first scenario of additional solar modules, the PI, IRR, NPV, PBP, and COE were 2.1, 5.46%, US$ 348.66, 11.7 years, and US$ cent 10.28/kWh, respectively. The typical temperatures were 47°C, 31°C, and 25°C for the inverter, radiator, and battery, respectively. The PV-supplied power was the highest, while the battery-supplied power was the lowest. The radiator temperature was highly correlated with the PV voltage, PV current, PV power, inverter current, and inverter power.

INDEX TERMS Energy, inverter efficiency, microgrid-interactive, monitored parameter, performance analysis.

I. INTRODUCTION

The demand for electrical energy has grown exponentially due to economic and industrialization development [1]. Therefore, it is necessary to use RESs due to clean sources [1]. When integrated into a grid, RESs require supplementary sources, such as other RESs, storage energy subsystems, and a DG for the continuous supply of power [1]. An EES subsystem significantly improves availability, stability, and efficiency [2], [3].

Solar energy is one type of abundant RES, with the most common energy conversion device of PV modules [1]. The PV module is simple, has less maintenance, no moving and rotating parts, and has zero noise and pollution [2]. Nevertheless, the output power depends on environmental factors, solar irradiance, weather conditions, and daylight duration [4], [5].

RESs involve using devices to measure, monitor, control, inform, communicate, manage and interact with technologies [6]. Batteries and DC-AC converters are also essential for RES integrations [1], [7]–[9] and influence a power flow [10].

Generally, studies regarding internal PV involve MPPT [11]–[26]. In addition, the studies are in the simulation stage [14], simulation and laboratory-scaled implementation stages [11], [15]–[17], [21], [22], [27] and laboratory-scaled implementation stages [12], [13], [18], [20], [23]–[26]. These studies could also be distinguished as standalone: static loaded [15], [17], BLDC-motor-loaded [18] and

The associate editor coordinating the review of this manuscript and approving it for publication was Bin Zhou.

SRM-loaded [23]; PV-grid connected [11], [13]–[15], [20], [22], PV-wind power plant-grid connected [11], [25], PV-fuel cell-grid connected [21], [27], PV-wind power plant-fuel cell-grid connected [16] and PV-wind power plant-battery-to-load connected [26]. A PV power plant also involves IoT technology, whether in concepts [28]–[30], prototype [24], concept and application [31] and application [32], including PV current, voltage, power and energy monitoring. PV grid integrations usually investigate inverters, especially concerning efficiency as a function of voltage [33]–[36] and power [34], [37]–[48].

Moreover, PV research has also been conducted in real applications. Usually, these studies involved one or a combination of design, implementation, performance, and economic analyses. The PV operation determines technical performance, expressed as a produced energy, PR, and efficiency [49]. A CF is an actual output energy ratio at a certain period to the amount of generated energy at a maximum power rating [50].

Sharma and Chandel [51] conducted research to acquire the RY, FY, PR, CF, efficiency, predicted and measured energy yields as technical performance. Kumar and Sudhakar [52] yielded FY, PR, CUF, and annual energy generation. Satsangi *et al.* [53] derived the PR and CF.

Another concern is economic analysis, which includes IRR, NPV, PI, PBP, LCC [54], and COE [54]–[56]. Kazem *et al.* [56] resulted in CF, annual yield factor, and COE. Emmanuel *et al.* [57] obtained FY, PR, LCOE, and PBP. Elamim, *et al.* [58] yielded the daily FY, PR, CF, LCOE, and PBP. Imam *et al.* [59] confirmed the CF, PR, LCOE, and NPV. Ibrik [60] obtained the FY, RY, CUF, and PR. The economic analysis also involved BEP and UEC [61], DPBT, LCOE, NPV [62], NPV and BEP, the unused and used interest rate of 6% [63], and cash flow and NPV versus years [64].

Regarding statistical analysis, the probability of PV power ramp rate [65], voltage, current, and power, on nonfault and fault versus sample time [66], and cumulative probability on mean LCOE and probability on SSR [67] were used for investigations. Moreover, the statistical tools of regression, mean, variance, and standard deviation [68], outlier detection rules [69], and standard deviation and kurtosis [70] were used for analyses.

The methods and results varied in various studies, areas, regions, and countries. Some points of view should be further studied. First, because PV grid integration uses the interactive configuration, some monitoring parameters should be increased, and the correlations among parameters should be analyzed using statistical tools. Moreover, the inverter efficiencies should also be sorted according to power flow categories. Scenarios on the year time of additional PV modules were also conducted to obtain some economic analysis options. These cases have gaps compared to previous studies.

In addition, most regions in Indonesia are geographically located along the equator; therefore, they obtain adequate sunshine year-round, thereby making it highly likely that they will build solar power generation systems [71].

Therefore, further research on solar power generation under real conditions is necessary for the implementation stage using more recording parameters that use IoT technology. Due to variations in power flow, the classifications of inverter efficiency must be investigated. Technical performance and some scenarios of economic analyses should also be conducted. Moreover, some statistical tools are necessary for analyzing the correlations and typical data among parameters.

The research contributions are daily PV and inverter voltage, current, and power, generated exported and imported energies, battery charge, and discharge energies, sorting inverter efficiencies, performance analysis, additional solar module scenarios of economic analysis, quartile ranges and typical power, voltages, currents, and temperatures and correlations among parameters.

This manuscript is divided into four sections. The introduction to renewable energy resources, solar power generation systems, and new ideas of the research are revealed in Section I. Furthermore, the research method is presented in Section II. The research results and discussions are included in Section III. Finally, the paper is concluded in Section IV.

II. MATERIALS AND RESEARCH METHOD

This research was carried out on the 1st building at ITENAS (Institut Teknologi Nasional Bandung), 23 PHH Mustafa Street, Bandung, Indonesia. As a short description of the location, Fig. 1(a) shows Bandung city on Java Island, Indonesia, and Fig. 1(b) shows the installed PV system located on the rooftop, with coordinates of 6°53'46.3''S and 107°38'10.2''E (-6.896186 and 107.636165).

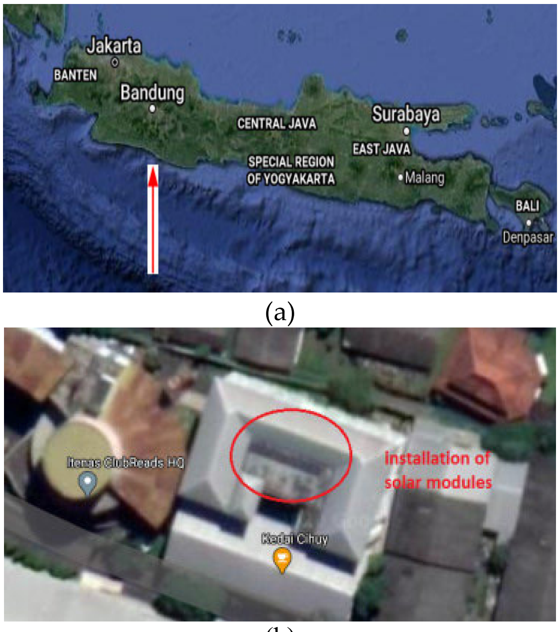

FIGURE 1. The location of the solar power plant installation, (a) Bandung on Java Island, (b) at Itenas campus.

First, the energy demand was determined to ensure that the supplied solar power was sufficient. Therefore, power usage was measured at intervals of 30 minutes from Monday to Sunday. Furthermore, the energy was computed by using the numerical integration of the composite trapezoidal rule, as shown in equation (1) [72].

$$\int_a^b f(x)\,dx \approx \frac{h}{2}\left[f(x_o) + 2\sum_{i=1}^{n-1} f(x_i) + f(x_n)\right] \tag{1}$$

The generated power depends on the solar module area, peak insolation, and solar module efficiency. Equation (2) [53] and equation (3) [53], [58] were used to determine the area and system efficiency, respectively.

$$A_a = \frac{P_{PVr}}{PSI\ x\ \eta_{PV}} \tag{2}$$

$$\eta_{sys} = \frac{E_{AC}}{A_a\ x\ H_t} \tag{3}$$

At the inverter input voltage rating of 200-600 volts, the configuration of the solar modules is in series [73]. Furthermore, to obtain an optimal output power, the direction of the modules was adjusted by using the tilted angle, as shown in equation (4) [73], [74].

$$Tilt\ angle = 90^\circ - latitude\ location \tag{4}$$

The system operates on-grid and off-grid methods; therefore, it was necessary to utilize a sufficient capacity of batteries to obtain an adequate power supply. By considering the DOD, the total capacity was determined by using equation (5) [75], [76].

$$I_{Aht} = \frac{I_{Ah}\ x\ day}{DOD} \tag{5}$$

Equation (6) was used to determine the number of battery units,

$$n_{bat} = \frac{I_{Aht}}{I_{Ah}} \tag{6}$$

The IoT-based metering system, through an Arduino controller integrated with the hybrid inverter, is shown in Fig. 2 as a schematic diagram. The inverter also includes SCC and MPPT. This system was not only voltage, current, power and energy on the PV, inverter and grid [32] but also on the battery, as well as the inverter, radiator and battery temperatures.

The energy of the solar irradiance is captured and converted to electrical energy by the solar modules in the forms of DC voltage, current, and power. These quantities enter the hybrid inverter as input. The second option is from the battery. The output quantities are AC voltage, current, power, and frequency. These parameters are also applicable to the grid. The load parameter is consumption power. Finally, the inverter, radiator, and battery temperatures are physical parameters.

The inverter, with battery storage, is used in the PV electrical generation system. The PV-produced energy will be optimized to maximize self-consumption. It can operate in time-of-use or auto and battery charge or discharge mode. In auto mode, the surplus PV energy will be charged into the battery. Otherwise, when PV energy is not sufficient, the inverter will discharge the battery energy to supply the local load. In a blackout case, the inverter operates in EPS mode, utilizing PV power and battery stored energy to supply the critical load.

The measurement results are stored in IC RTC DS1307. A Raspberry pi is used as a device to transmit the measured data to the cloud. Data acquisition is automatically conducted in real time.

The estimated generated energy of the solar modules is determined by equation (7) [77], [78].

$$E_{daily-est} = Insolation\left(\frac{kWh/m^2}{day}\right) x\ A_m\left(m^2\right) x\ \eta_{PV}\ x\ f_{dirt}\ x\ f_{cable} \tag{7}$$

The inverter efficiency indicates the converted DC-to-AC power, as shown in equation (8) [52].

$$\eta_{inv} = \frac{P_{AC}}{P_{DC}}\ x\ 100\% \tag{8}$$

The system performance was evaluated based on the IEC 61724 standard, such as RY (Y_R), FY (Y_F), PR, CF, and system efficiency. These values were calculated by using equations (9) up to (13) [50]–[52], [54], [58]–[60], [79]–[81].

$$Y_R = \frac{H_t}{H_R} \tag{9}$$

$$Y_F = \frac{E_{AC}}{P_{PVr}} \tag{10}$$

$$P_R = \frac{Y_F}{Y_R} \tag{11}$$

$$CF = \frac{E_{AC}}{P_{PVr}\ x\ (24h/d)\ x\ (day\ number)} \tag{12}$$

$$\eta_{sys} = \frac{E_{AC}}{H_t\ x\ A_m}\ x\ 100\% \tag{13}$$

An economic analysis is necessary to determine the profit of installing a solar power generation system. The LCC was determined by equation (14) [59], [82].

$$LCC = S + O\&M \tag{14}$$

The PBP and PI were calculated using equations (15) [60] and (16) [82], respectively.

$$PBP = \frac{investment}{net\ income} \tag{15}$$

$$PI = \frac{present\ value\ of\ future\ cash flow}{initial\ investment} \tag{16}$$

The NPV and IRR were calculated using equations (17) and (18), respectively [83].

$$NPV = \sum_{t=0}^{n} \frac{NCF_t}{(1+k)^t} \tag{17}$$

$$NPV = \sum_{t=0}^{n} \frac{NCF_t}{(1+IRR)^t} = 0 \tag{18}$$

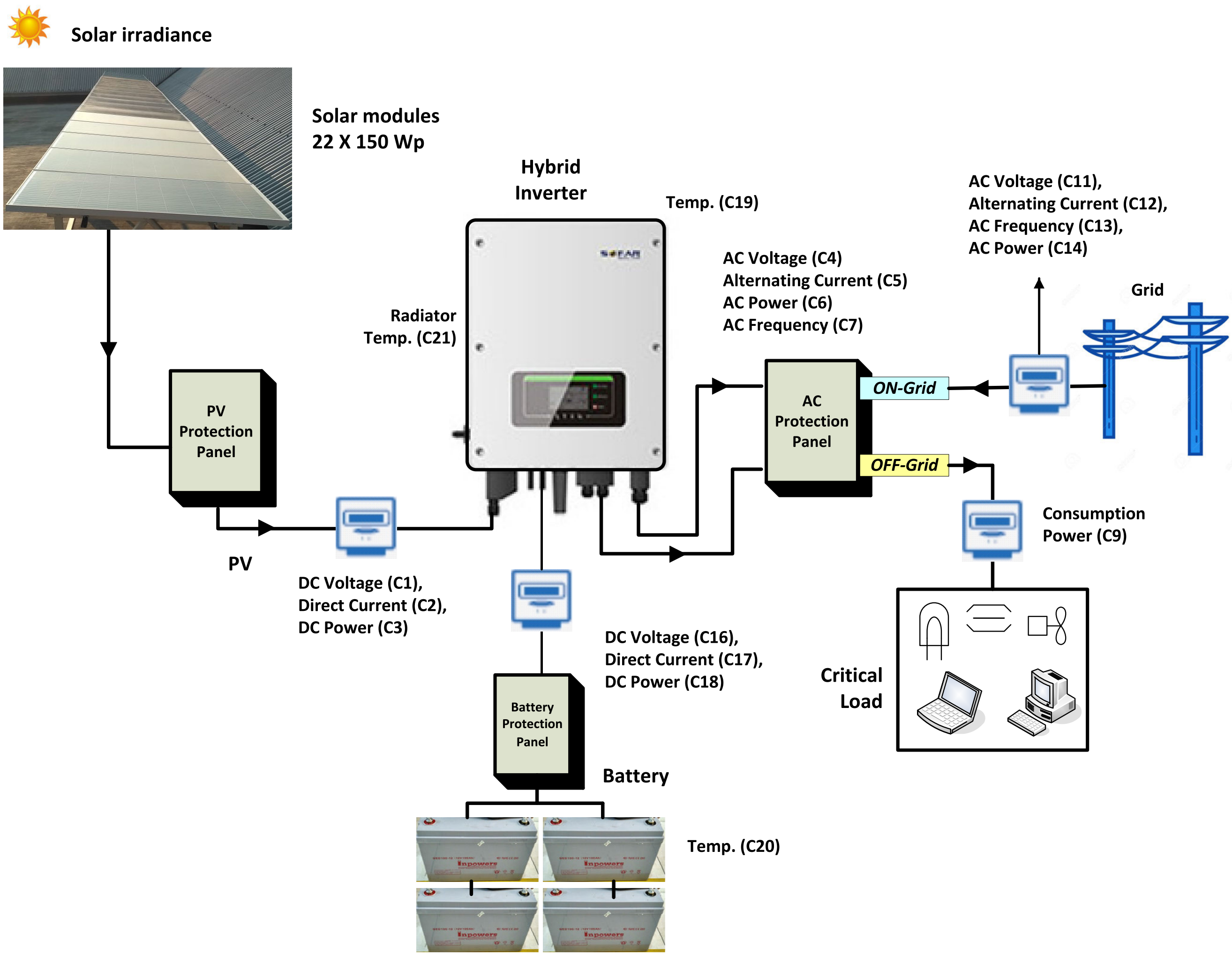

FIGURE 2. Implemented grid-interactive schematic diagram.

Finally, the COE was determined by equation (19) [56], [57].

$$COE = \frac{LCC}{\sum_{1}^{n} E_{PV}} \tag{19}$$

Box plots, PCA, and correlation coefficients were involved in the analysis of typical values and parameter closeness of recorded data [84], [85]. Due to power and time accumulation, the energy was analyzed separately.

III. RESULTS AND DISCUSSION

Fig. 3(a) shows the loading power patterns for seven days with an interval measurement of 30 minutes. Fig. 3(b) shows the consumed energy per day. From Monday to Friday, the consumed energy was in the range of 11-15 kWh, while for Saturday and Sunday, the consumed energy was zero. This case indicated that the lecture room load was only effective on working days with a total consumed energy of 65.92 kWh and a maximum demand energy of 14.55 kWh.

TABLE 1. Estimated PV-generated energy.

Dates	Predicted energy (kWh)	Cumulative predicted energy (kWh)
11- 30 Nov.	14.11	290.48
1-20 Dec.	15.31	306.12
Total predicted energy		**596.60**

The estimation of the produced energy in one day was determined using equation (7), as listed in Table 1, for 40 days of the experimental duration. This period was chosen because there were some weather variations, such as sunny, rainy, temperate, and cloudy conditions visually. Therefore, basically, this period represented a year condition. Based on NASA surface meteorology and solar energy, the effective insolations for November and December 2019 were 4.59 kWh/m^2/day and 4.83 kWh/m^2/day, respectively [86]. The area of installed solar modules and their efficiency are assumed to be 22 m^2 and 15%, respectively. The loss factors due to dirt (f_{dirt}) and cabling (f_{cable}) are 0.97 and 0.99, respectively [87].

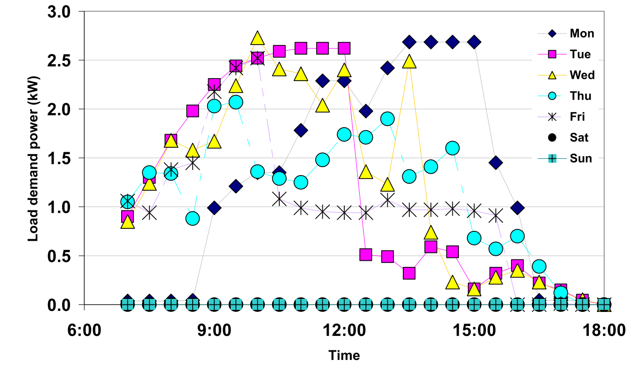

(a)

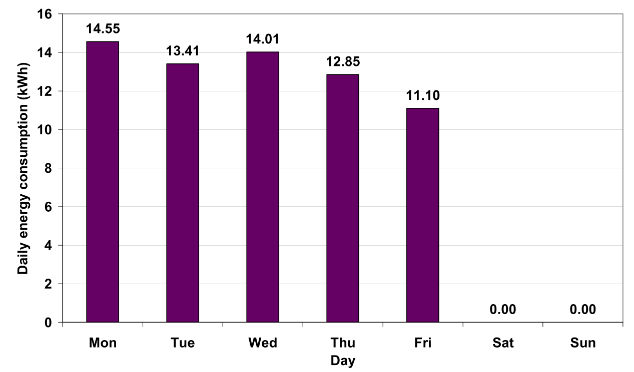

(b)

FIGURE 3. Grid daily load consumed (a) power, and (b) energy.

(a)

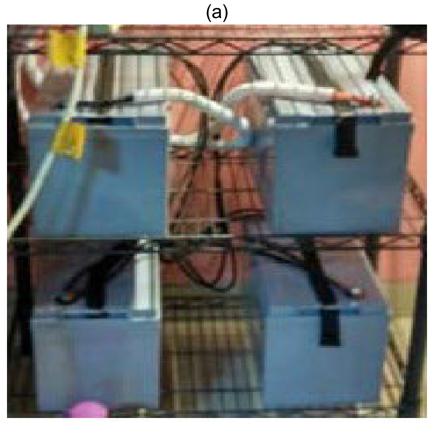

(b)

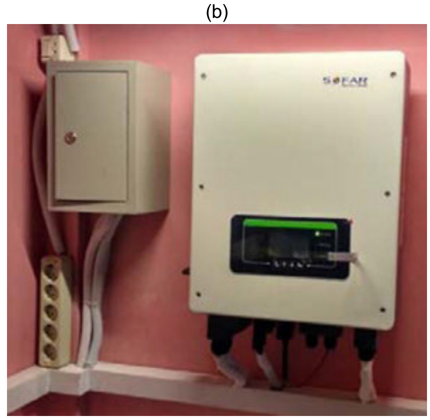

(c)

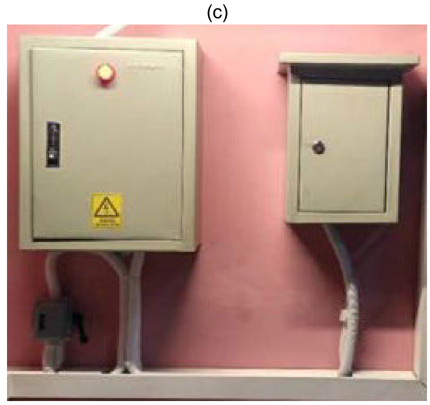

(d)

FIGURE 4. Main components of the implemented microgrid-interactive configuration; (a) solar modules, (b) battery units, (c) battery protection panel and hybrid inverter, (d) PV and AC protection panels.

The 22 × 150 Wp solar modules, a total of 3.3 kWp, were installed on a rooftop, as shown in Fig. 4(a). The angle of tilt was determined by using equation (4) to be 83.08 degrees, leaning north permanently. Battery units of 4 × 100 Ah are used for energy storage, as shown in Fig. 4(b). The hybrid inverter connects the solar modules and grid (on-grid) to the battery and load (off-grid), as shown in Fig. 4(c). Finally, the system is equipped with battery, PV, and grid protection panels, as shown in Figs. 4(c) and 4(d). Table 2 lists the specifications of the main equipment on the solar modules, hybrid inverter, and battery.

Fig. 5(a) shows the sample charts of the voltage and current on the solar modules on November 16, 2019. The output peak current and voltage were 8.31 amperes and 428.1 volts, respectively. Fig. 5(b) shows the chart of the output power of the solar modules with a 2.97 kW peak. Fig. 5(c) shows the inverter output voltage and current with a maximum of 238.5 volts and 11.71 amperes. Fig. 5(d) shows the peak inverter output power of 2.92 kW. The power and current chart patterns were typical. However, the PV voltage pattern was rather different from the inverter voltage due to battery existence.

Fig. 6 shows the daily generated energy for the 40 days, with the largest value of 21.20 kWh, on 16 November 2019. The computation-based estimated and actual measurement-based generated energies were 596.60 kWh and 550.00 kWh, respectively, a difference of 46.6 kWh or 7.81%. The average

TABLE 2. Specifications of main equipment.

Solar modules	
Module type	Polycrystalline
Maximum power (W)	150
Optimum power voltage (V)	18.61
Optimum operating current (A)	8.06
Open circuit voltage (V)	22.19
Short circuit current (A)	8.62
Module efficiency (%)	15.12
Hybrid inverter	
Max. input power (W)	6,600
Max. DC input voltage (V)	600
Start-up DC voltage (V)	120
Full load DC voltage range (V)	300-520
MPPT number	2
Max. DC input current (A)	12
Max. output power (W)	6000
Max. output current (A)	27.3
Nominal grid voltage (V)	220, 230, 240
Nominal grid frequency (Hz)	44-55
AC voltage range (V)	180-276
EPS rated power (W)	3000
EPS nominal voltage (V)	230
EPS nominal frequency (Hz)	50/60
EPS rated current (A)	13
Switch time (ms)	10
Battery type	Lead-Acid, Lithium Ion
Nominal battery voltage (V)	48
Max. charge current (A)	60
Max. discharge current (A)	70
Battery recommended (Ah)	100-500
Battery DOD (%)	Lithium:0-80 Lead acid:0-50
Battery	
Type	Lead-Acid
Nominal voltage (V)	12
Nominal capacity (Ah)	100
Max. discharge current (A)	1200 (5s)
Internal resistance (mΩ)	4.9
Max. charge current	0.1C

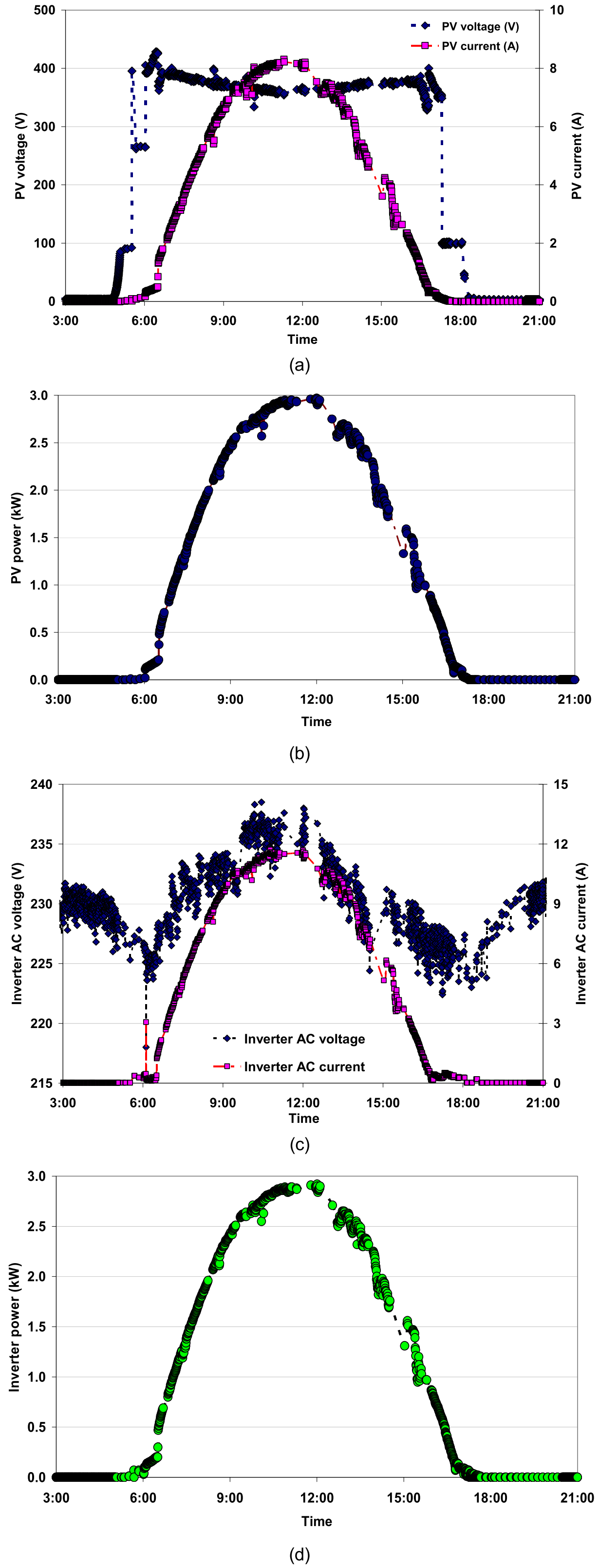

FIGURE 5. PV and inverter output charts; (a) PV voltage and current, (b) PV power, (c) inverter voltage and current, and (d) inverter power.

irradiation time of the generated energy measurement was 4.7 hours.

Fig. 7 shows the chart of load energy consumption. The average consumed energy was 6.58 kWh, and in 40 days, it amounted to 263.30 kWh.

Fig. 8 shows the exported and imported energies, which are indicated by positive and negative signs, respectively. The total exported and imported energies were 278.30 kWh and 7.70 kWh, or 97.31% and 2.69%, respectively. Thus, the exported energy was much higher than the imported energy.

The battery charge and discharge energies varied greatly depending on the system condition, as shown in Fig. 9. The total energy used to charge the battery was 45.20 kWh. The total energy to send the load was 38.70 kWh. Therefore, the charge and discharge portions of energy were 53.87% and 46.13%, respectively.

Based on the total solar irradiation, the average solar irradiance was 4.91 kWh/m^2/day. The total sun radiation for the 40 days was 196.4 kWh/m^2 with an RY of 196.4 kWh/kWp.

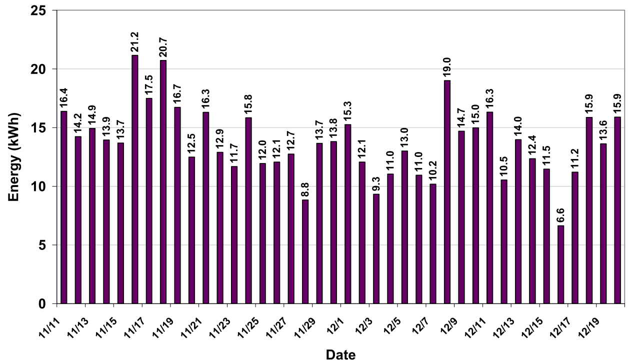

FIGURE 6. Daily generated energy.

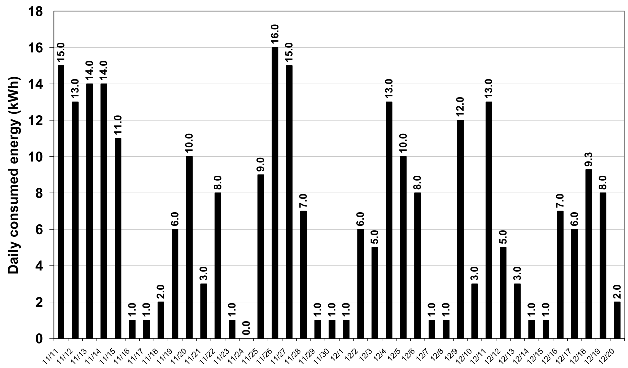

FIGURE 7. Load consumed energy.

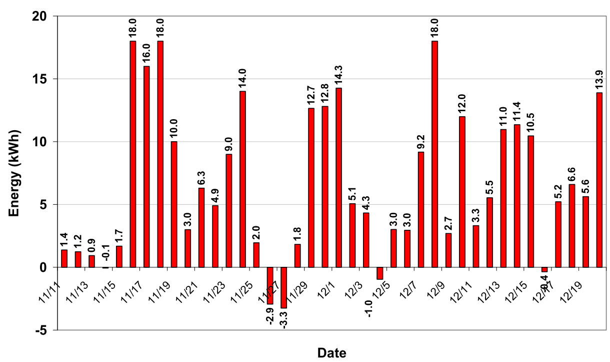

FIGURE 8. Chart of exported and imported energies.

Because the total output energy for the 40 days was 550.00 kWh and the PV rating was 3.3 kWp, the FY was 166.70 kWh/kWp. The PR was 84.80% based on the FY and RY. As it is compared, this value was slightly higher than the finding by Ayompe *et al.*, the annual average of 81.5%, with the range of 72.3-91.6% [50], Sharma and Chandel, 55-84% [51], Emmanuel *et al.*, 76-79% [57], Elamim *et al.*, 82% [58], Imam *et al.*, 78% [59], and considerably higher than the finding by Satsangi *et al.*, 63% [53]. Nevertheless, it is lower than that found by Kumar and Sudhakar, 86.12% [52], and Ibrik, 88%, 86%, and 85% [60].

Based on the output energy and the FY, the CF was 17.36%. This value is higher than that by Ayompe *et al.*, 5.0-15.5% [50], Satsangi *et al.*, 9% [53], Sharma and Chandel, 9.27% [51], and Emmanuel *et al.*, 12.5% [57] but lower than that by Kazem *et al.*, 21.7% [56], Elamim *et al.*, 21.56% and 21.93% [58], Imam *et al.*, 22% [59], and Al-Waeli *et al.*, 17.82-25.52% [81]. This value is also in line with the range of 0.16-0.26 for fixed slope type solar power generation systems [76].

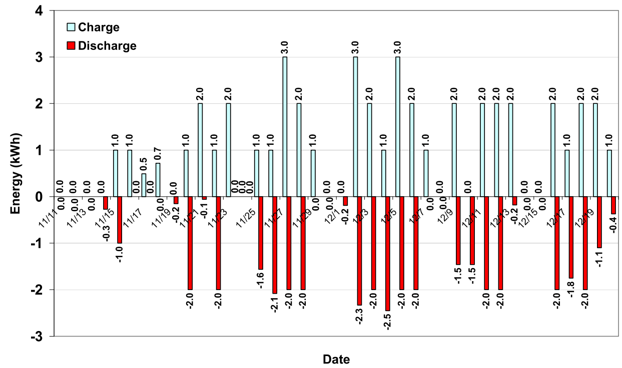

FIGURE 9. Battery charge and discharge energies.

While the system efficiency was 12.73%, this value is higher than the value of Sharma and Chandel, 8.3% [51], Satsangi *et al.*, 8.51% [53], and Al-Waeli *et al.*, 9.1% [81], close to the value by Ayompe *et al.*, 11.3-14.3% [50], Emmanuel *et al.*, 11.71-12.19% [57], and Elamim *et al.*, 10.59-13.60% and 10.20-13.73% [58], lower than the value by Ibrik, 13.7% [60]. Thus, the yielded parameters were slightly more and less than those in previous studies. This research had higher system efficiency than some previous studies.

The classifications of power flow in some categories, as the new research contribution, are when the PV produced power as equal (or close) to the load consumed power, greater than the load consumed power, less than the load consumed power, greater than the load consumed power with the full battery, in no-load and loaded conditions, and less than the load demand power with a low capacity of batteries as first to sixth categories, respectively.

In the first category, the overall power was used by the load, whereas the batteries were in a static condition, as shown in Fig. 10(a).

Fig. 10(b) shows the power patterns on January 30, 2020, which indicates that the PV power flowed to the load. The PV modules produced average input and output powers of 1590 watts and 1570 watts, respectively. Practically, the power was neither exported nor imported to the grid. The battery units were neither charged nor discharged. This condition occurred from 13:00-15:00 with produced and load consumption energies of 13 kWh and 10 kWh, respectively. Therefore, the surplus energy of 3 kWh was exported to the grid. The typical closeness was ± 100 watts tolerance.

In the second category, excess power is used to charge the batteries, where the SOC is less than 100%. This category is shown in Fig. 11(a). The PV-generated power flowed to

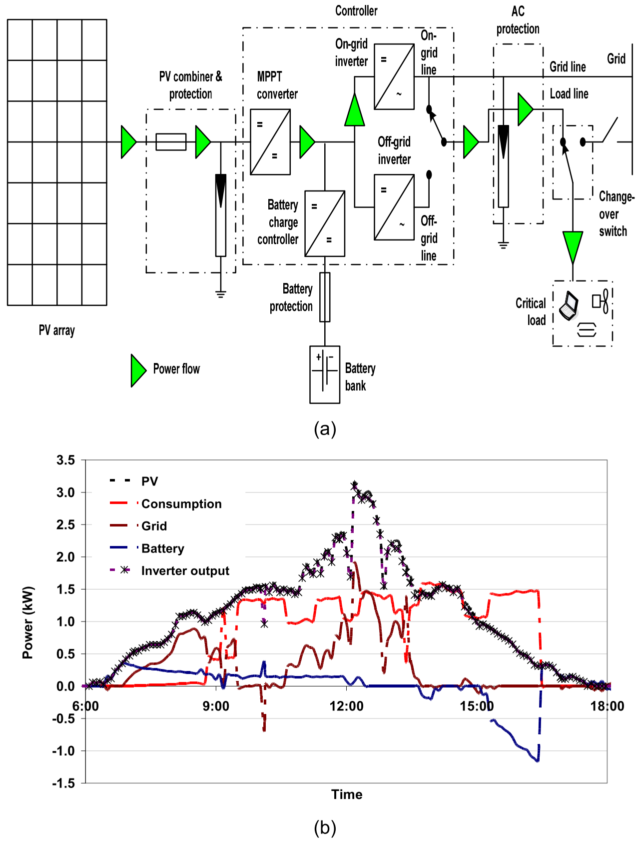

FIGURE 10. **PV produced power (a) flow (b) chart, close to the load consumed power.**

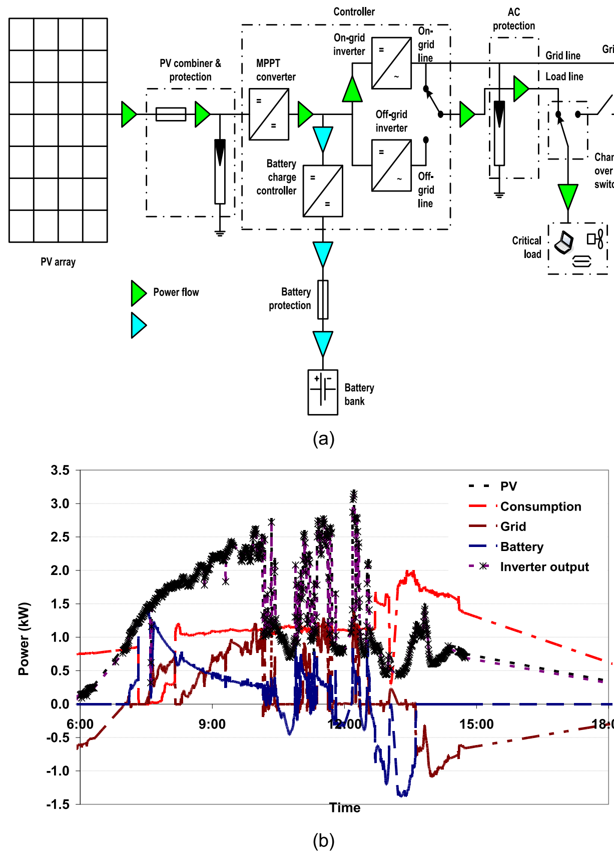

FIGURE 11. **PV produced power (a) flow and (b) chart, greater than consumed power.**

the load according to the consumption and as part of battery charging. The observed chart is shown in Fig. 11(b) on November 27, 2019. The load consumption was smaller than the PV-produced power, with an average of 937 watts. Meanwhile, the PV modules produced average input and output powers of 1731 watts and 1698 watts, respectively. Excess PV power was used as the battery charging, with an average of 600 watts. Additionally, the chart shows the presence of more PV module-produced power, which was exported to the grid, at an average of 382 watts. This condition occurred from 07:00 to 12:30, thereby producing a total energy of 12.74 kWh.

In the third category, the PV produced power was less than the load consumed power with the shortage supplied by the battery, as shown in Fig. 12(a). The battery capacity should be higher than the specified DOD. Fig. 12(b) is the chart of the sample on December 16, 2019.

The average load consumed, PV module, and inverter powers were 1378 watts, 846 watts, and 828.7 watts, respectively. However, the load required additional supply from the batteries because the PV-produced power was less than the load consumed, with an average power of -539 watts (discharge). This condition occurred from 08:30 to 11:30, with the ability to fulfill the load power by the PV modules and batteries, as long as the DOD was 80%, and this category produced a total energy of 6.64 kWh and consumed energy of 7.00 kWh.

The fourth and fifth categories show that the PV produced power is greater than the load demand, with batteries of 100% SOC. Therefore, the excess produced energy was exported to the grid, as shown in Fig. 13.

The fourth and fifth categories are distinguished by no loaded and loaded conditions, as shown in Figs. 14(a) and 14(b), respectively. These samples of patterns were taken on November 16, 2019 (a) and January 8, 2020 (b). On the first chart, the peak PV, average, and inverter produced power was 2900 watts, 1840 watts, and 1803 watts, respectively. All PV-produced power was exported to the grid because the system did not supply load and the battery capacity was 100% SOC. Nevertheless, in the second chart, the load consumption was smaller than the PV power. The PV, average, and inverter, as well as the load consumed powers, were 3000 watts, 1747 watts, 1707 watts, and 536 watts, respectively. The average power, which was not consumed by the load, was exported to the grid as 413 positive watts because there was no charging on the battery. The produced energy was (a) 21.16 kWh and (b) 11.37 kWh, while the total energy consumption of scheme (b) was 6 kWh. Therefore, it saved surplus energy that was exported to the grid of 5.37 kWh.

In the sixth category, the PV produced power is less than the load demand with insufficient battery capacity, as shown

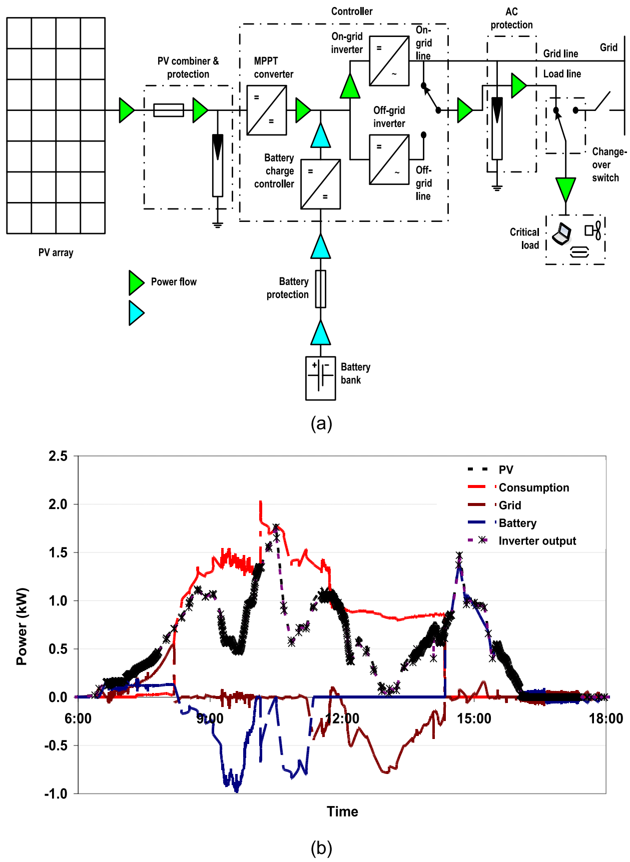

FIGURE 12. PV-produced power (a) flow and (b) chart, less than consumed power.

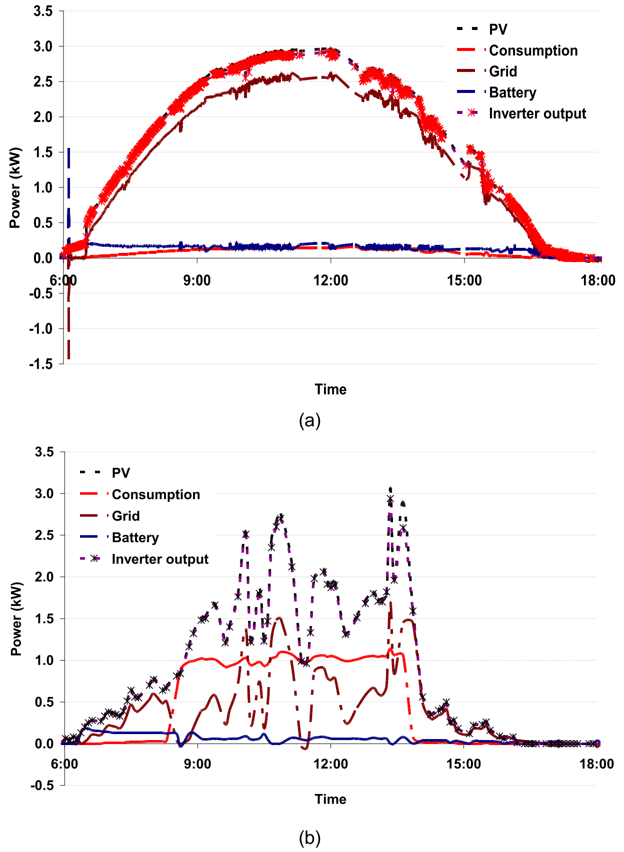

FIGURE 14. PV produced power (a) no-load, and (b) loaded conditions greater than consumed power.

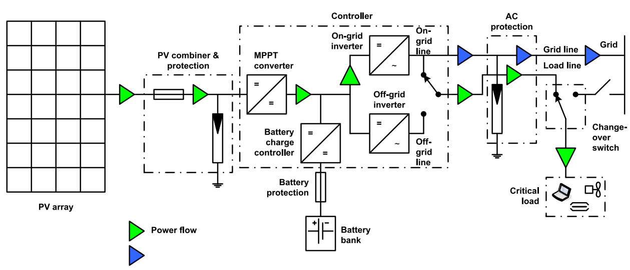

FIGURE 13. Power flow of PV produced power greater than load demand, with batteries of 100% SOC.

in Fig. 15(a). Therefore, the system imported the shortage power from the grid on the load consumption, with the charts shown in Fig. 15(b). The average load, PV, and inverter consumed powers were 1568 watts, 540 watts, and 494 watts, respectively. The load lacked power was -1111 watts (negative). This condition was taken on February 13, 2020 and occurred from 13:00 to 17:00.

The typical inverter efficiencies for the first to sixth categories are shown in Fig. 16. Undoubtedly, the typical efficiencies on the first, second, fourth, and fifth categories were fairly close, between 95% and 98%, as the first group was due to the PV main power supply to the load. The third and sixth categories were moderately different from the previous categories because the PV-produced power was lower than the load demand. The inverter efficiencies lied between 90% and 95%, as the second group.

These typical inverter efficiencies were relatively close to the annual average values, which resulted from Ayompe *et al.*, 89.2% [50], Satsangi *et al.*, 90.9% [53], the optimum efficiency yielded by Kazem *et al.*, 94.65% [56], the monthly inverter efficiency range of 94.9-95.7%, Emmanuel *et al.* [57], and Ibrik, 92.5% [60].

The EPS occurs when the inverter is not connected to the grid, and the load depends solely on the solar modules and batteries. Unfortunately, under these conditions, the electrical parameters were not recorded due to no Wi-Fi signal.

Table 3 lists the initial investment costs of the solar generation equipment. It did not meet economic feasibility, so it is necessary to add solar modules. There were three scenarios of an additional 22 solar modules in the planning of the first, fifth or tenth year, bringing the total capacity to 6.6 kWp. Therefore, there is an additional investment cost in that year of USD 2,625.26. This plant is assumed to operate for 25 years. The batteries are replaced periodically every 5 years. The hybrid inverter is carried out periodically every 5 years at 10% of the cost to keep the system working reliably and efficiently. The costs are US$ 3,032.43 and 2,779.73 for four battery replacements and four hybrid

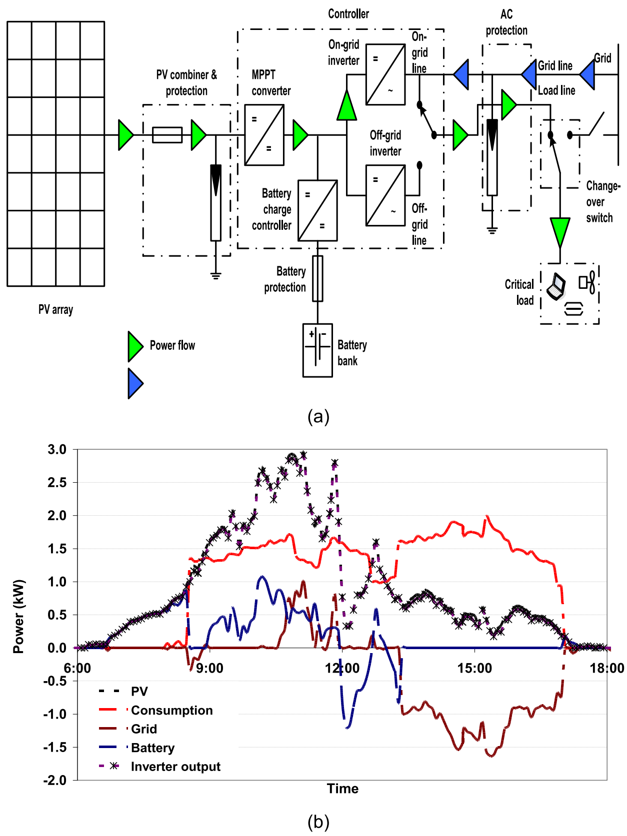

FIGURE 15. PV produced power (a) flow, and (b) chart, less than consumed power, low battery capacity.

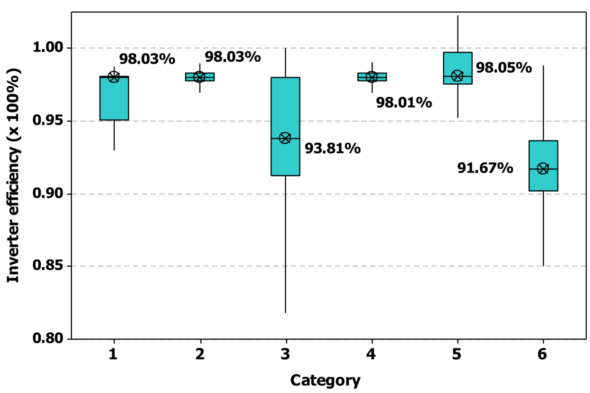

FIGURE 16. Categories of inverter efficiency.

inverter maintenance devices, respectively. A maintenance cost is necessary to ensure that the solar modules are free of dirt to work properly, set at US$ 10.53, for one day in one month. Thus, for 25 years, the total maintenance cost is US$ 3,159. The total expenditure is US$ 8,971.16. The LCC is the initial investment added to the total expenditures during the operation, US$ 16,692.60.

Table 4 shows the summary of economic analysis for the scenarios of additional solar modules as a further contribution. The first scenario is economically feasible, so economic

TABLE 3. Initial investment costs.

No	Description	Quantity (pcs, set, ls)	Unit cost (US$)	Total cost (US$)
1	Polycrystalline PV module 150 Wp	22	119.33	2,625.26
2	Hybrid inverter 6 kW	1	2,316.44	2,316.44
3	Battery 100Ah, 12 V	4	189.53	758.12
4	Protective equipment and off-grid wires	3	252.70	758.10
5	PV module holders	3	210.59	631.77
6	On-grid wires	1	126.35	126.35
7	Battery rack	1	84.23	84.23
8	Installation cost	3	140.39	421.17
	Grand total			7,721.44

TABLE 4. Summary of economic analysis for the scenarios.

Parameters	Original (Scen. 0)	Additional solar modules		
		1st year (Scen. 1)	5th year (Scen. 2)	10th year (Scen. 3)
Initial investment cost (US$)	7,721.44	7,721.44	7,721.44	7,721.44
Additional investment cost (US$)	0	(in 1st y) 2,625.26	(in 5th y) 2,625.26	(in 10th y) 2,625.26
Battery replacement cost (US$)	3,032.43	3,032.43	3,032.43	3,032.43
Hybrid inverter maintenance cost (US$)	2,779.73	2,779.73	2,779.73	2,779.73
Equipment replacement cost (US$)	8,971.16	8,971.16	8,971.16	8,971.16
Income for 25-year operation (US$)	12,641.70	25,810.14	23,703.19	21,069.50
NPV (US$)	-4,073.21	348.66	-293.89	-1,785.45
IRR (%)	-0.113	5.46	-1.92	-3.10
PBP (years)	29.8	11.7	12.6	15.3
PI	0.83	2.1	1.97	1.63
COE (cent US$)	13.82	10.28	10.28	10.28

analysis was carried out. The payback period is 11.7 years; in the ranges by Zhang *et al.*, [55], 6.5, 6.7, 17.6, and 16.8 years, depending on SCR, longer than that yielded in studies by Kazem *et al.*, [56], 10 years, Emmanuel *et al.*, [57], 6.4 years, and Al-Waeli *et al.* [81], 8 years, but shorter than that by Elamim *et al.*, [58], 12 years, and Imam *et al.*, [59], 14.6 years.

According to the Decree of the Minister of Energy and Mineral Resources of the Republic of Indonesia 55K of 2019, the applicable national cost of supply was US$ cent 7.86/kWh (IDR 1,119/kWh), and the local cost in West Java was US$ cent 6.91/kWh (IDR 984). Since the purchase price is determined by agreement, it is assumed that the purchase of electricity is the same as the national cost of supply, at US$ cent 7.86/kWh.

The amount of energy calculated as income came from the amount of energy generated by the system based on the rating capacity and the exposure durations of sun radiation. The data on the exposure duration of solar radiation were obtained from the Meteorology, Climatology, and Geophysics Agency for a period of one year. Therefore, the generated energy

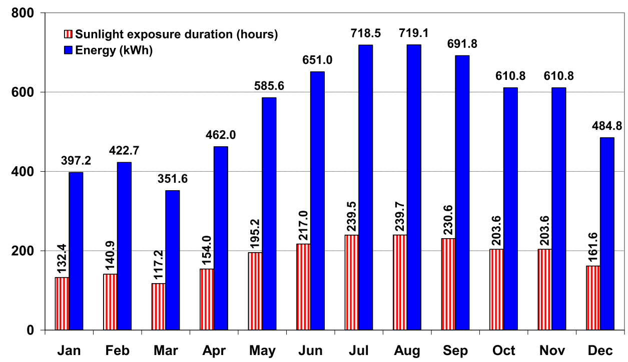

FIGURE 17. Generated energy based on the sunlight exposure duration.

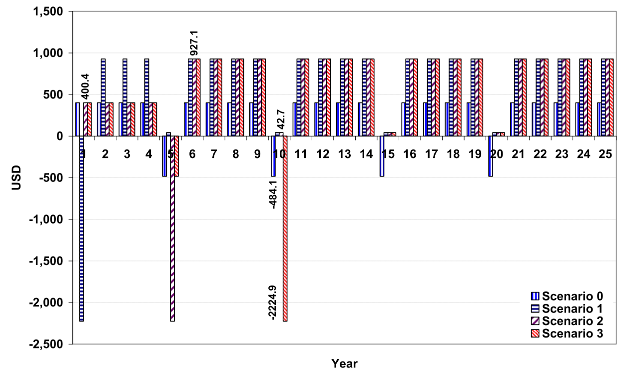

FIGURE 18. Net cash flows.

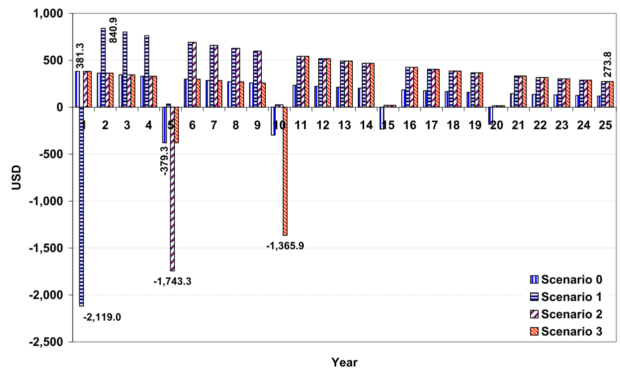

FIGURE 19. Present values.

TABLE 5. Life cycle cost per year.

No	Description	Cost (USD)	Time (years)	Annual Cost (USD)
1	Polycrystalline PV modules 150 Wp	5,250.52	25	210.02
2	Hybrid inverter 6000 watts	2,316.44	5	463.29
3	Battery 100Ah, 12 V	758.12	5	151.62
4	Protective equipment and off-grid wires	758.10	25	30.32
5	PV module holders	631.77	25	25.27
6	On-grid wires	126.35	25	5.05
7	Battery rack	84.23	25	3.37
8	Installation cost	421.17	25	16.85
9	Maintenance cost	3,158.78	25	126.35
	TOTAL			1,032.14

is shown in Fig. 17, where the total energy and the duration of solar radiation for one year are 6,705.9 kWh and 2,235.3 hours, respectively.

The cost of electrical energy is a comparative calculation of the predetermined energy price and obtains the profitability index, which is 1. The COE based on the LCC requires component and maintenance costs of US$ 1,032.14, as listed in Table 5. The total generated energy in one year is 10,035.66 kWh. Thus, the COE can be found as US$ cent 10.28/kWh. Therefore, it is still higher than the cost set by the Minister of Energy and Mineral Resources. This value is less than those of previous studies, such as 0.2-0.43 €/kWh, by Silva and Hendrick [78], 0.2258 US$/kWh, by Kazem *et al.*, [56], 12.1, 14.1 and 16.2 C/kWh for 4%, 6%, and 8% discount rates, by Emmanuel *et al.* [57] and by Al-Waeli *et al.*, 0.196 USD/kWh [81], but higher than that proposed by Elamim *et al.*, 0.068 €/kWh (≈0.08 US$/kWh) [58] and by Imam *et al.*, 0.0382 $/kWh [59].

Fig. 18 shows the net cash flow without an additional solar module in scenario 0 and with three additional solar modules in the first, fifth and tenth years in scenarios 1, 2, or 3, with a cost of US$ 2,224.9, while the nominal net cash flow is US$ 927.1.

Furthermore, Fig. 19 shows the present values for four scenarios, i.e., without an additional solar module, as in scenario 0, and additional solar modules in the first, fifth and tenth years as in scenarios 1, 2, and 3, respectively. Of course, generally, the present values will decrease as the year increases. Generally, the lowest present values are in scenario 0 due to no additional energy produced by the solar modules. Consequently, it is not any additional PV power or energy. Indeed, the highest present value in the second year is scenario 1 (first scenario), US$ 840.9, due to the additional 22 solar modules in the first year.

Moreover, the last new unique research contribution was statistical analysis of the recorded data. Fig. 20(a) shows the mean powers for the photovoltaic output, inverter output, consumption, grid, and batteries as 499.9 watts, 484.9 watts, 250.8 watts, 199.7 watts, and 32.0 watts, respectively. The PV and inverter output powers are the highest values and ranges. The interquartile ranges are 790 watts and 760 watts, between 0 and 790 watts, and between 0 and 760 watts for the PV and inverter output powers, respectively. These ranges, as the first group, were quite high due to the high fluctuation of the solar irradiance. The average consumption and grid powers were 250.8 watts and 199.7 watts, respectively, outside the interquartile ranges of 100 watts and 60 watts. These ranges occupied the second group due to loading

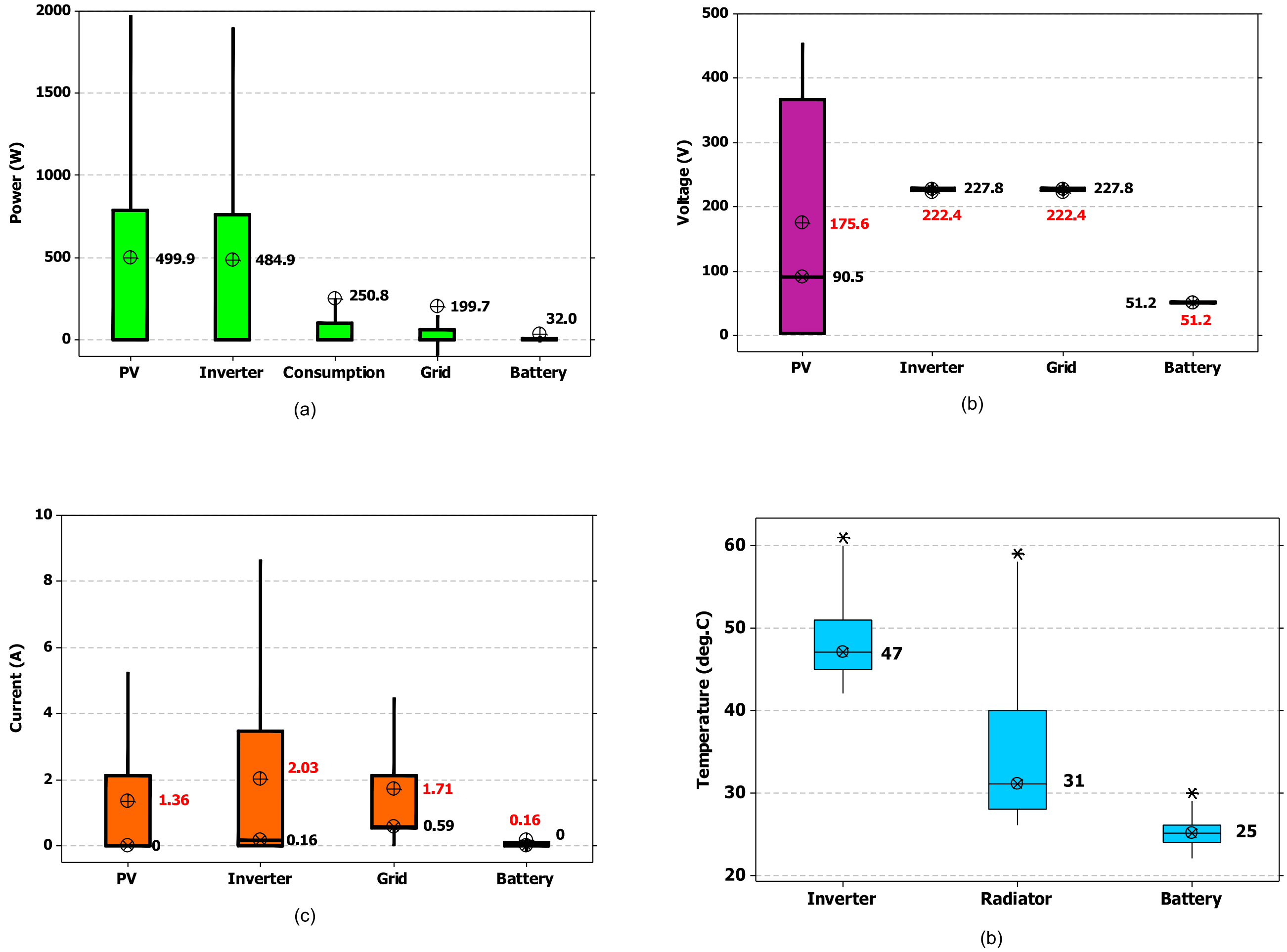

FIGURE 20. **(a) Range and average power, (b) range, typical and average voltages, (c) currents, and (d) temperatures.**

variation. The average battery power was 32 watts, outside the interquartile range of 10 watts. The output power of the batteries was the lowest among the parameters. This case indicated that the battery has backup power.

Fig. 20(b) shows the typical and average voltages for the photovoltaic, inverter, grid, and battery. The PV voltage variation was the highest, with an interquartile range of 363.9 volts, between 3.5 volts and 367.4 volts, and median and mean values of 90.5 volts and 175.6 volts, respectively. Indeed, this case was caused by very high fluctuations in solar irradiance, from midnight to noon. The inverter and grid voltages were the same, as small voltage variations, with interquartile ranges of 4.8 volts, between 225 volts and 229.8 volts, and the median and mean values were 227.8 volts and 222.4 volts, respectively. The inverter and grid voltages need to be the same. The battery voltages had very small variations, with interquartile ranges of 1.7 volts, between 50.3 volts and 52.0 volts, and both median and mean values of 51.2 volts.

Fig. 20(c) shows the ranges, means, and medians of the currents on the PV, inverter, grid, and battery. The average currents were 1.36 A, 2.03 A, 1.71 A, and 0.16 A, respectively, for the PV, inverter, grid, and batteries. While their interquartile ranges were 2.11 A, 3.45 A, 1.58 A, and 0.1 A, respectively. Thus, the highest current, at once, the highest current range, was for the inverter due to the loading. The PV current was lower than the current of the inverter due to the higher voltage and higher voltage range. The battery current occupied the lowest and lowest current ranges due to backup, not as the main power source.

Fig. 20(d) shows the typical temperatures of the inverter, radiator, and battery, which are 47°C, 31°C, and 25°C, respectively. There were some temperature spikes in each component, 61°C, 59°C, and 30°C, as statistical outliers. Indeed, the highest temperatures were for the inverter because it suffered from a loading current in the main components of the semiconductor, with an interquartile range of 6°C and between 45°C and 51°C. The second-highest temperatures were for the radiator because this component is outside and close to the inverter. The interquartile range was 12°C, between 28°C and 40°C. The lowest temperatures were for the battery, with an interquartile range of 2°C and between

TABLE 6. Correlation coefficients among parameters.

	C1	C2	C3	C4	C5	C6	C7	C9	C11	C12	C13	C14	C16	C17	C18	C19	C20
C2	**0.680**																
C3	**0.687**	**0.999**															
C4	-0.027	0.037	0.030														
C5	**0.672**	**0.962**	**0.961**	0.019													
C6	**0.686**	**0.999**	**0.999**	0.029	**0.961**												
C7	0.031	0.019	0.019	0.186	0.019	0.019											
C9	0.480	**0.571**	**0.573**	-0.044	**0.662**	**0.572**	0.014										
C11	-0.027	0.037	0.030	**1.000**	0.019	0.029	0.186	-0.044									
C12	**0.537**	**0.787**	**0.783**	0.102	**0.769**	**0.783**	0.016	0.203	0.102								
C13	0.031	0.019	0.019	0.186	0.019	0.019	**1.000**	0.014	0.186	0.016							
C14	0.431	**0.748**	**0.744**	0.094	**0.712**	**0.744**	0.011	-0.053	0.094	**0.836**	0.011						
C16	**0.517**	**0.521**	**0.525**	0.009	0.421	**0.530**	-0.007	-0.044	0.009	0.485	-0.007	**0.592**					
C17	0.060	0.148	0.152	-0.014	-0.121	0.154	0.002	-0.304	-0.014	0.056	0.002	0.120	0.379				
C18	0.181	0.259	0.265	-0.040	-0.005	0.269	0.005	-0.207	-0.040	0.136	0.005	0.180	0.457	**0.979**			
C19	**0.705**	**0.663**	**0.662**	-0.093	**0.690**	**0.663**	-0.013	0.495	-0.093	**0.564**	-0.013	0.441	0.422	-0.088	0.035		
C20	0.105	0.098	0.096	-0.109	0.123	0.096	-0.040	0.156	-0.109	0.067	-0.040	0.009	0.064	-0.086	-0.053	**0.609**	
C21	**0.740**	**0.748**	**0.747**	-0.078	**0.768**	**0.750**	-0.004	**0.521**	-0.078	**0.642**	-0.004	**0.522**	0.488	-0.066	0.073	**0.977**	0.491

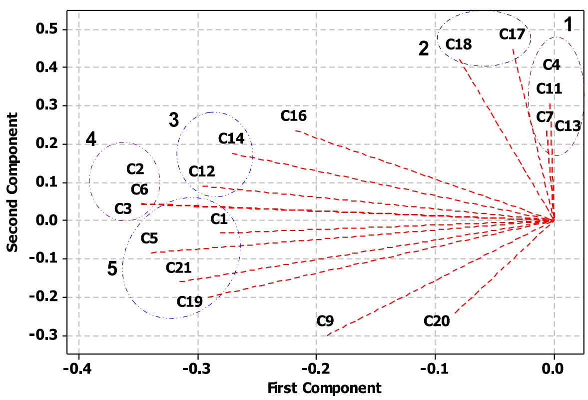

FIGURE 21. Principal component analysis of microgrid parameters.

24°C and 26°C. They were very rarely discharged and loaded.

Fig. 21 shows the PCA among parameters. It is classified into five groups because of the closeness of one variable to another. The first group is the grid frequency (C13), grid voltage (C11), inverter voltage (C4), and inverter frequency (C7), which are positively correlated. Increasing one parameter value was followed by three remaining parameters. The second group is the battery current (C17) and battery power (C18). Indeed, the battery power increased, and the current also increased. The third group is the grid power (C14) and grid current (C12). Of course, the grid power increased as the grid current increased. Furthermore, the fourth group is the PV current (C2), inverter power (C6), and PV power (C3). The inverter increase was followed by PV power and current. Finally, the fifth group consisted of the PV voltage (C1), inverter current (C5), radiator temperature (C21), and inverter temperature (C19). Thus, increasing the PV voltage and inverter current raise both the inverter and radiator temperatures.

Table 6 lists the correlation coefficients among parameters. They are sorted into five categories: very high correlation (0.9-1.0), high correlation (0.7-0.9), moderate correlation (0.4-0.7) and low correlation (0.2-0.4) and slight correlation (under 0.2) [88]. The first category, as the most correlated, is between PV current (C2) and the PV power (C3), inverter current (C5) and inverter power (C6), between PV power (C3) and the inverter current (C5), and inverter power (C6), between the inverter current (C5) and inverter power (C6), between the inverter voltage (C4) and grid voltage (C11), between the inverter frequency (C7) and grid frequency (C13), between the battery current (C17) and battery power (C18), and between inverter temperature (C19) and the radiator temperature (C21).

Moreover, the second categories were between the PV voltage (C1) and inverter (C19) and radiator (C21) temperatures, between PV current (C2) and grid current (C12) and grid power (C14), between the PV power (C3) and grid current (C12), grid power (C14) and radiator temperature (C21), between the inverter current (C5) and the grid current (C12), grid power (C14), inverter temperature (C19) and radiator temperature (C21), between the inverter power (C6) and grid current (C12), grid power (C14) and radiator temperature (C21), and between the grid current (C12) and grid power (C14). Of course, the radiator temperature had a very high correlation with the inverter temperature. The remaining correlations generally included moderate, low, or slight correlations.

As an emphasis, these figures used PCA and correlation coefficient analysis of statistical tools for a PV electrical power generation system, as new ideas comparing previous studies, such as ramp rate [65], voltage, current and power versus time on fault and no-fault conditions [66], LCOE and SSR probability [67], regression, mean, variance and standard deviation [68], outlier detection rules [69] and standard deviation and kurtosis [70].

IV. CONCLUSION

The developed IoT-based PV microgrid-interactive configuration operates properly. Based on the experimental measurements for 40 days, the load consumed, total exported energy, total imported energy, battery charging energy, and total battery expended energy for load feeding were 263.30 kWh, 278.30 kWh, 7.70 kWh, 45.20 kWh, and 38.70 kWh, respectively. The total estimated computations of the generated and measured energies were 596.60 kWh and 550.00 kWh, respectively, with a difference of 7.81%.

The system PR, CF, and efficiency were 84.8%, 17.36%, and 12.73%, respectively. The typical inverter efficiencies for the PV produced power close to the load consumed power, greater than load power, less than the load power, greater than load power, with 100% battery SOC, for no-load and loaded, and lower than load power, low battery was 98.03%, 98.03%, 93.81%, 98.01%, 98.05%, and 91.67%, respectively. The lower PV-produced power resulted in a slightly lower inverter efficiency.

By the scenario of 22 additional solar modules in the first year, the NPV is positive, US$ 348.66. The PI is 2.1, more than 1, and the IRR is 5.46%, which is greater than the prevailing interest rate (5%). The PBP is 11.7 years, from the estimated operating time of 25 years. The system is economically feasible, with a COE of US$ cent 10.28/kWh, higher than the price set by the Minister of Energy and Mineral Resources Regulation, US$ cent 7.86/kWh.

The PV and inverter output powers had high interquartile ranges, between 0 and 790 watts and between 0 and 760 watts, respectively. The voltage range was the highest for PV, with an interquartile range between 3.5 volts and 367.4 volts. The typical inverter, radiator, and battery temperatures were 47°C, 31°C, and 25°C, respectively. The inverter temperature was highly correlated with PV voltage. The radiator temperature was highly correlated with the PV voltage, PV current, PV power, inverter current, and inverter power. The radiator temperature was very highly correlated with the inverter temperature.

APPENDIX

NOMENCLATURE

ACRONYM

BEP	break even time
BLDC	brushless DC
C	cent
CF	capacity factor (%)
COE	cost of energy (US$/kWh)
CUF	capability utilization factor (%)
DG	diesel generator
DOD	depth of discharge (%)
DPBT	discounted payback time
EES	electrical energy storage
EPS	emergency power supply
FY	final yield (Y_F) (kWh/kWp)
IoT	internet of things
IRR	internal rate of return (%)
kWh	kilowatt hour
kWp	kilowatt peak
LCC	life cycle cost (US$)
LCOE	levelized cost of energy (US$/kWh)
MPPT	maximum power point tracking
NASA	National Aeronautics and Space Administration
NPV	net present value (US$)
O & M	operational and maintenance costs (US$)
PBP	payback period (year)
PCA	principal component analysis
PI	profitability index
PR	performance ratio (P_R) (%)
PV	photovoltaic
RES	renewable energy source
RY	reference yield (Y_R) (kWh/kWp)
SCC	solar charge controller
SCR	self-consumption rate
SOC	state of charge
SRM	switched reluctance motor
SSR	self-sufficiency ratio (%)
UEC	unit electrical cost

CURRENCY

US$	United States dollar ($, USD)
€	Euro
IDR	Indonesian rupiah (1$=IDR 14,246)

NOTATION

C1	PV voltage (V)
C2	PV current (A)
C3	PV power (W)
C4	inverter voltage (V)
C5	inverter current (A)
C6	inverter power (W)
C7	inverter frequency (Hz)
C9	consumption power (W)
C11	grid voltage (V)
C12	grid current (A)
C13	grid frequency (Hz)
C14	grid power (W)
C16	battery voltage (V)
C17	battery current (A)
C18	battery power (W)
C19	inverter temperature (°C)
C20	battery temperature (°C)
C21	radiator temperature (°C)

PARAMETER

a	lower limit of integral
A_a	installed solar module area (m^2)
A_m	total area of installed solar modules (m^2)
b	upper limit of integral
E_{AC}	AC output energy (kWh)
E_{PV}	PV output energy (kWh)
$f(x_0)$	lower limit function

$f(x_i)$	i^{th} function
$f(x_n)$	upper limit function
f_{cable}	cabling factor
f_{dirt}	dirty factor
h	step size
H_R	reference irradiance (kW/m^2)
H_t	total insolation (kWh/m^2)
I_{Ah}	battery capacity (Ah)
I_{Aht}	total battery capacity (Ah)
k	discount rate (%)
n_{bat}	number of battery units
$NCFt$	t^{th} year net income (US$)
n_{PV}	number of installed solar modules
P_{AC}	inverter output power (kW)
P_{DC}	inverter input power (kW)
P_{PVr}	PV rating power (kW_p)
PSI	peak insolation (W/m^2)
S	initial investment cost (US$)
η_{inv}	inverter efficiency (%)
η_{PV}	PV module efficiency (%)
η_{sys}	system efficiency (%)

REFERENCES

[1] I. Yahyaoui, *Advances in Renewable Energies and Power Technologies: Solar and Wind Energies*, vol. 1, Amsterdam, The Netherlands: Elsevier, 2018, pp. 23–25.

[2] J. P. Ram and N. Rajasekar, "Design of PV systems with battery storage," in *Smart Grid Systems, Modeling, and Control*, N. R. Babu Ed. Waretown, NJ, USA: Apple Academic, 2019, pp. 11–40.

[3] S. Ruin and G. Sidén, *Small-Scale Renewable Energy Systems: Independent Electricity for Community, Business and Home*. Leiden, The Netherlands: CRC Press/Balkema, 2020, pp. 117–127.

[4] V. Caballero, D. Vernet, A. Zaballos, and G. Corral, "Prototyping a web-of-energy architecture for smart integration of sensor networks in smart grids domain," *Sensors*, vol. 18, pp. 1–25, Jan. 2018.

[5] G. Boyle, *Renewable Electricity and the Grid, The Challenge of Variability*. London, U.K.: Earthscan, 2007, pp. 1–29.

[6] B. Shakerighadi, A. A. Moghaddam, J. C. Vasquez, and J. M. Guerrero, "Internet of Things for modern energy systems: State-of-the-art, challenges, and open issues," *Energies*, vol. 11, pp. 1–23, May 2018.

[7] S. Rauf and N. Khan, "Application of DC–AC hybrid grid and solar photovoltaic generation with battery storage using smart grid," *Int. J. Photoenergy*, vol. 2017, pp. 1–16, Sep. 2017.

[8] M. H. Mahlooji, H. R. Mohammadi, and M. Rahimi, "A review on modeling and control of grid-connected photovoltaic inverters with LCL filter," *Renew. Sustain. Energy Rev.*, vol. 81, pp. 563–578, Jan. 2018.

[9] C. C. Gomes, A. F. Cupertino, and H. A. Pereira, "Damping techniques for grid-connected voltage source converters based on LCL filter: An overview," *Renew. Sustain. Energy Rev.*, vol. 81, pp. 116–135, Jan. 2018.

[10] M.-A. Rodríguez-Licea, F.-J. Perez-Pinal, A.-G. Soriano-Sánchez, and J.-A. Vázquez-López, "Noninvasive vehicle-to-load energy management strategy to prevent li-ion batteries premature degradation," *Math. Problems Eng.*, vol. 2019, pp. 1–9, May 2019.

[11] N. Priyadarshi, S. Padmanaban, P. K. Maroti, and A. Sharma, "An extensive practical investigation of FPSO-based MPPT for grid integrated PV system under variable operating conditions with anti-islanding protection," *IEEE Syst. J.*, vol. 13, no. 2, pp. 1861–1871, Jun. 2019.

[12] N. Priyadarshi, S. Padmanaban, M. Sagar Bhaskar, F. Blaabjerg, and A. Sharma, "Fuzzy SVPWM-based inverter control realisation of grid integrated photovoltaic-wind system with fuzzy particle swarm optimisation maximum power point tracking algorithm for a grid-connected PV/wind power generation system: Hardware implementation," *IET Electr. Power Appl.*, vol. 12, no. 7, pp. 962–971, Aug. 2018.

[13] N. Priyadarshi, K. Yadav, V. Kumar, and M. Vardia, "An experimental study on zeta buck-boost converter for application in PV system," in *Handbook of Distributed Generation Electric Power Technologies, Economics and Environmental Impacts*. Cham, Switzerland: Springer, 2017, pp. 393–406.

[14] N. Priyadarshi, A. K. Sharma, and S. Priyam, "An experimental realization of grid-connected PV system with MPPT using dSPACE DS 1104 control board," in *Advances in Smart Grid and Renewable Energy*. Singapore: Springer, 2018, pp. 125–133.

[15] N. Priyadarshi, A. K. Sharma, and S. Priyam, "Practical realization of an improved photovoltaic grid integration with MPPT," *Int. J. Renew. Ener. Res.*, vol. 7, no. 4, pp. 1880–1891, Dec. 2017.

[16] N. Priyadarshi, A. K. Sharma, and F. Azam, "A hybrid firefly-asymmetrical fuzzy logic controller based MPPT for PV-wind-fuel grid integration," *Int. J. Renew. Energy Res.*, vol. 7, pp. 1546–1560, Dec. 2017.

[17] N. Priyadarshi, A. Anand, A. Sharma, F. Azam, V. Singh, and R. Sinha, "An experimental implementation and testing of GA based maximum power point tracking for PV system under varying ambient conditions using dSPACE DS 1104 controller," *Int. J. Renew. Ener. Res.*, vol. 7, no. 1, pp. 255–256, Mar. 2017.

[18] N. Priyadarshi, S. Padmanaban, L. Mihet-Popa, F. Blaabjerg, and F. Azam, "Maximum power point tracking for brushless DC motor-driven photovoltaic pumping systems using a hybrid ANFIS-FLOWER pollination optimization algorithm," *Energies*, vol. 11, pp. 1–16, Apr. 2018.

[19] N. Priyadarshi, F. Azam, A. K. Bhoi, and S. Alam, "An artificial fuzzy logic intelligent controller based MPPT for PV grid utility," in *Proc. 2nd Int. Conf. Commun., Comput. Netw. (ICCCN)*, Singapore: Springer, 2019, pp. 901–909.

[20] S. Padmanaban, N. Priyadarshi, J. B. Holm-Nielsen, M. S. Bhaskar, F. Azam, A. K. Sharma, and E. Hossain, "A novel modified sine-cosine optimized MPPT algorithm for grid integrated PV system under real operating conditions," *IEEE Access*, vol. 7, pp. 10467–10477, 2019.

[21] S. Padmanaban, N. Priyadarshi, M. S. Bhaskar, J. B. Holm-Nielsen, E. Hossain, and F. Azam, "A hybrid photovoltaic-fuel cell for grid integration with Jaya-based maximum power point tracking: Experimental performance evaluation," *IEEE Access*, vol. 7, pp. 82978–82990, 2019.

[22] N. Priyadarshi, S. Padmanaban, J. B. Holm-Nielsen, F. Blaabjerg, and M. S. Bhaskar, "An experimental estimation of hybrid ANFIS–PSO-based MPPT for PV grid integration under fluctuating sun irradiance," *IEEE Syst. J.*, vol. 14, no. 1, pp. 1218–1229, Mar. 2020.

[23] N. Priyadarshi, M. S. Bhaskar, S. Padmanaban, F. Blaabjerg, and F. Azam, "New CUK–SEPIC converter based photovoltaic power system with hybrid GSA–PSO algorithm employing MPPT for water pumping applications," *IET Power Electron.*, vol. 13, no. 13, pp. 2824–2830, Oct. 2020.

[24] N. Priyadarshi, S. Padmanaban, J. B. Holm-Nielsen, M. S. Bhaskar, and F. Azam, "Internet of Things augmented a novel PSO-employed modified zeta converter-based photovoltaic maximum power tracking system: Hardware realisation," *IET Power Electron.*, vol. 13, no. 13, pp. 2775–2781, Oct. 2020.

[25] N. Priyadarshi, S. Padmanaban, D. M. Ionel, L. Mihet-Popa, and F. Azam, "Hybrid PV-wind, micro-grid development using quasi-Z-source inverter modeling and control-experimental investigation," *Energies*, vol. 11, pp. 1–15, Aug. 2018.

[26] N. Priyadarshi, V. K. Ramachandaramurthy, S. Padmanaban, and F. Azam, "An ant colony optimized MPPT for standalone hybrid PV-wind power system with single Cuk converter," *Energies*, vol. 12, pp. 1–23, Jan. 2019.

[27] N. Priyadarshi, S. Padmanaban, M. S. Bhaskar, F. Blaabjerg, J. B. Holm-Nielsen, F. Azam, and A. K. Sharma, "A hybrid photovoltaic-fuel cell-based single-stage grid integration with Lyapunov control scheme," *IEEE Syst. J.*, vol. 14, no. 3, pp. 3334–3342, Sep. 2020.

[28] E. Kabalci and Y. Kabalci, *From Smart Grid to Internet of Energy*. London, U.K.: Academic, 2019 pp. 249–307.

[29] A. R. Di Fazio, T. Erseghe, E. Ghiani, M. Murroni, P. Siano, and F. Silvestro, "Integration of renewable energy sources, energy storage systems, and electrical vehicles with smart power distribution networks," *J. Ambient Intell. Humanized Comput.*, vol. 4, no. 6, pp. 663–671, May 2013.

[30] K. Huang, L. Shu, K. Li, F. Yang, G. Han, X. Wang, and S. Pearson, "Photovoltaic agricultural Internet of Things towards realizing the next generation of smart farming," *IEEE Access*, vol. 8, pp. 76300–76312, Apr. 2020.

[31] E. K. Lee, W. Shi, R. Gadh, and W. Kim, "Design and implementation of a microgrid energy management system," *Sustainability*, vol. 8, pp. 1–19, Nov. 2016.

[32] P. de Arquer Fernández, M. Á. Fernández Fernández, J. L. C. Candás, and P. A. Arboleya, "An IoT open source platform for photovoltaic plants supervision," *Int. J. Electr. Power Energy Syst.*, vol. 125, Feb. 2021, Art. no. 106540.
[33] L. T. Scarabelot, C. R. Rambo, and G. A. Rampinelli, "A relative power-based adaptive hybrid model for DC/AC average inverter efficiency of photovoltaics systems," *Renew. Sustain. Energy Rev.*, vol. 92, pp. 470–477, Sep. 2018.
[34] G. A. Rampinelli, A. Krenzinger, and F. C. Romero, "Mathematical models for efficiency of inverters used in grid connected photovoltaic systems," *Renew. Sustain. Energy Rev.*, vol. 34, pp. 578–587, Jun. 2014.
[35] Z. Salam and A. A. Rahman, "Efficiency for photovoltaic inverter: A technological review," in *Proc. IEEE Conf. Energy Convers. (CENCON)*, Oct. 2014, pp. 175–180.
[36] F. Wu, X. Li, F. Feng, and H. B. Gooi, "Modified cascaded multilevel grid-connected inverter to enhance European efficiency and several extended topologies," *IEEE Trans. Ind. Informat.*, vol. 11, no. 6, pp. 1358–1365, Dec. 2015.
[37] P. M. Rodrigo, R. Velázquez, and E. F. Fernández, "DC/AC conversion efficiency of grid-connected photovoltaic inverters in central Mexico," *Sol. Energy*, vol. 139, pp. 650–665, Dec. 2016.
[38] V.-G. Gerardo, M.-R. P. Raymundo, and S.-Z. J. Miguel, "High efficiency single-phase transformer-less inverter for photovoltaic applications," *Ingeniería, Investigación y Tecnología*, vol. 16, no. 2, pp. 173–184, Apr./Jun. 2015.
[39] Y. Ando, T. Oku, M. Yasuda, K. Ushijima, H. Matsuo, and M. Murozono, "Dependence of electric power flow on solar radiation power in compact photovoltaic system containing SiC-based inverter with spherical Si solar cells," *Heliyon*, vol. 6, no. 1, Jan. 2020, Art. no. e03094.
[40] P. M. Rodrigo, D. L. Talavera, E. F. Fernández, F. M. Almonacid, and P. J. Pérez-Higueras, "Optimum capacity of the inverters in concentrator photovoltaic power plants with emphasis on shading impact," *Energy*, vol. 187, Nov. 2019, Art. no. 115964.
[41] Q. Huang, A. Q. Huang, R. Yu, P. Liu, and W. Yu, "High-efficiency and high-density single-phase dual-mode cascaded buck–boost multilevel transformerless PV inverter with GaN AC switches," *IEEE Trans. Power Electron.*, vol. 34, no. 8, pp. 7474–7488, Aug. 2019.
[42] M. Islam and S. Mekhilef, "Efficient transformerless MOSFET inverter for a grid-tied photovoltaic system," *IEEE Trans. Power Electron.*, vol. 31, no. 9, pp. 6305–6316, Sep. 2016.
[43] F. Spertino, F. Corona, and P. Di Leo, "Limits of advisability for master–slave configuration of DC–AC converters in photovoltaic systems," *IEEE J. Photovolt.*, vol. 2, no. 4, pp. 547–554, Oct. 2012.
[44] M. H. Ahmed, M. Wang, M. A. S. Hassan, and I. Ullah, "Power loss model and efficiency analysis of three-phase inverter based on SiC MOSFETs for PV applications," *IEEE Access*, vol. 7, pp. 75768–75781, 2019.
[45] J.-S. Kim, J.-M. Kwon, and B.-H. Kwon, "High-efficiency two-stage three-level grid-connected photovoltaic inverter," *IEEE Trans. Ind. Electron.*, vol. 65, no. 3, pp. 2368–2377, Mar. 2018.
[46] R. González, E. Gubía, J. López, and L. Marroyo, "Transformerless single-phase multilevel-based photovoltaic inverter," *IEEE Trans. Ind. Electron.*, vol. 55, no. 7, pp. 2694–2702, Jul. 2008.
[47] F. B. Grigoletto, "Five-level transformerless inverter for single-phase solar photovoltaic applications," *IEEE J. Emerg. Sel. Topics Power Electron.*, vol. 8, no. 4, pp. 3411–3422, Dec. 2020.
[48] Y.-H. Kim, Y.-H. Ji, J.-G. Kim, Y.-C. Jung, and C.-Y. Won, "A new control strategy for improving weighted efficiency in photovoltaic AC module-type interleaved flyback inverters," *IEEE Trans. Power Electron.*, vol. 28, no. 6, pp. 2688–2699, Jun. 2013.
[49] N. Pearsall, *The Performance of Photovoltaic (PV) Systems Modelling, Measurement and Assessment*. Duxford, U.K.: Elsevier, 2017, pp. 135–208.
[50] L. M. Ayompe, A. Duffy, S. J. McCormack, and M. Conlon, "Measured performance of a 1.72kW rooftop grid connected photovoltaic system in Ireland," *Energy Convers. Manage.*, vol. 52, no. 2, pp. 816–825, Feb. 2011.
[51] V. Sharma and S. S. Chandel, "Performance analysis of a 190 kWp grid interactive solar photovoltaic power plant in India," *Energy*, vol. 55, pp. 476–485, Jun. 2013.
[52] B. Shiva Kumar and K. Sudhakar, "Performance evaluation of 10 MW grid connected solar photovoltaic power plant in India," *Energy Rep.*, vol. 1, pp. 184–192, Nov. 2015.
[53] K. P. Satsangi, D. B. Das, G. S. S. Babu, and A. K. Saxena, "Performance analysis of grid-interactive solar photovoltaic plant in India," *Energy Sust. Dev.*, vol. 47, pp. 9–16, Dec. 2018.
[54] N. Sommerfeldt and H. Madani, "Revisiting the techno-economic analysis process for building-mounted, grid-connected solar photovoltaic systems: Part one—Review," *Renew. Sustain. Energy Rev.*, vol. 74, pp. 1379–1393, Jul. 2017.
[55] Y. Zhang, T. Ma, P. E. Campana, Y. Yamaguchi, and Y. Dai, "A techno-economic sizing method for grid-connected household photovoltaic battery systems," *App. Energy*, vol. 269, Jul. 2020, Art. no. 115106.
[56] H. A. Kazem, M. H. Albadi, A. H. A. Al-Waeli, A. H. Al-Busaidi, and M. T. Chaichan, "Techno-economic feasibility analysis of 1 MW photovoltaic grid connected system in Oman," *Case Stud. Thermal Eng.*, vol. 10, pp. 131–141, Sep. 2017.
[57] M. Emmanuel, D. Akinyele, and R. Rayudu, "Techno-economic analysis of a 10 kWp utility interactive photovoltaic system at Maungaraki school, Wellington, New Zealand," *Energy*, vol. 120, pp. 573–583, Feb. 2017.
[58] A. Elamim, B. Hartiti, A. Haibaoui, A. Lfakir, and P. Thevenin, "Comparative study of photovoltaic solar systems connected to the grid: Performance evaluation and economic analysis," *Energy Procedia*, vol. 159, pp. 333–339, Feb. 2019.
[59] A. A. Imam and Y. A. Al-Turki, "Techno-economic feasibility assessment of grid-connected PV systems for residential buildings in Saudi Arabia–A case study," *Sustainability*, vol. 12, pp. 1–25, Dec. 2019.
[60] I. H. Ibrik, "Techno-economic assessment of on-grid solar PV system in Palestine," *Cogent Eng.*, vol. 7, Feb. 2020, Art. no. 1727131.
[61] C. O. C. Oko, E. O. Diemuodeke, N. F. Omunakwe, and E. Nnamdi, "Design and economic analysis of a photovoltaic system: A case study," *Int. J. Renew. Energy Dev.*, vol. 1, no. 3, pp. 65–73, Oct. 2012.
[62] F. Cucchiella, I. D'Adamo, and M. Gastaldi, "Economic analysis of a photovoltaic system: A resource for residential households," *Energies*, vol. 10, pp. 1–15, Jun. 2017.
[63] J. Windarta, A. Nugroho, and B. Bagaskoro, "Design and analysis of technical economics of off-grid systems solar power plant using Homer at cemara island, brebes regency," in *Proc. 4th Int. Conf. Energy, Env., Epid. Inf. Syst. (ICENIS)*, Semarang, Indonesia, Aug. 2019, pp. 1–6.
[64] C. D. M. Affonso and M. Kezunovic, "Technical and economic impact of PV-BESS charging station on transformer life: A case study," *IEEE Trans. Smart Grid*, vol. 10, no. 4, pp. 4683–4692, Jul. 2019.
[65] M. K. Hossain and M. H. Ali, "Statistical analysis of ramp rates of solar photovoltaic system connected to grid," in *Proc. IEEE Energy Convers. Congr. Expo. (ECCE)*, Sep. 2014, pp. 2524–2531.
[66] M. Mansouri, M. Hajji, M. Trabelsi, M. F. Harkat, A. Al-khazraji, A. Livera, H. Nounou, and M. Nounou, "An effective statistical fault detection technique for grid connected photovoltaic systems based on an improved generalized likelihood ratio test," *Energy*, vol. 159, pp. 842–856, Sep. 2018.
[67] D. Coppitters, W. De Paepe, and F. Contino, "Robust design optimization and stochastic performance analysis of a grid-connected photovoltaic system with battery storage and hydrogen," *Energy*, vol. 213, pp. 1–14, Dec. 2020.
[68] H. A. Kazem, M. T. Chaichan, A. H. A. Al-Waeli, and K. Sopian, "A novel model and experimental validation of dust impact on grid-connected photovoltaic system performance in Northern Oman," *Sol. Energy*, vol. 206, pp. 564–578, Aug. 2020.
[69] Y. Zhao, F. Balboni, T. Arnaud, J. Mosesian, R. Ball, and B. Lehman, "Fault experiments in a commercial-scale PV laboratory and fault detection using local outlier factor," in *Proc. IEEE 40th Photovoltaic Spec. Conf. (PVSC)*, Jun. 2014, pp. 3398–3403.
[70] S. Shedd, B.-M. Hodge, A. Florita, and K. Orwig, "A statistical characterization of solar photovoltaic power variability at small timescales," in *Proc. 2nd Ann. Int. Workshop Integ. Sol. Power Power Syst. Conf.*, Lisbon, Portugal, Nov. 2012, pp. 1–6.
[71] R. Syahputra and I. Soesanti, "Renewable energy systems based on micro-hydro and solar photovoltaic for rural areas: A case study in Yogyakarta, Indonesia," *Energy Rep.*, vol. 7, pp. 472–490, Nov. 2021.
[72] J. H. Mathews, *Numerical Methods for Mathematics, Science, and Engineering*, 2nd ed. Englewood Cliffs, NJ, USA, Prentice-Hall, 1992, pp. 357–366.
[73] R. Mayfield, *Photovoltaic Design & Installation for Dummies*, Indianapolis, IN, USA; Wiley, 2010, pp. 90–92.
[74] M. Boxwell, *Solar Electricity Handbook*, 11th ed. Birmingham, U.K.: Greenstream, 2017, pp. 44–73.
[75] C. V. Nayar, M. Ashari, and W. W. L. Keerthipala, "A grid-interactive photovoltaic uninterruptible power supply system using battery storage and a back up diesel generator," *IEEE Trans. Energy Convers.*, vol. 15, no. 3, pp. 348–353, Sep. 2000.

[76] G. M. Masters, *Renewable and Efficient Electric Power Systems*, 2nd ed. Hoboken, NJ, USA: Wiley, 2013, p. 303.
[77] S. M. Ahsan, H. A. Khan, N. Hassan, S. M. Arif, and T. T. Lie, "Optimized power dispatch for solar photovoltaic-storage system with multiple buildings in bilateral contracts," *Appl. Energy*, vol. 273, pp. 1–16, Sep. 2020.
[78] G. de Oliveira e Silva and P. Hendrick, "Photovoltaic self-sufficiency of Belgian households using lithium-ion batteries, and its impact on the grid," *Appl. Energy*, vol. 195, pp. 786–799, Jun. 2017.
[79] S. Yadav, S. K. Panda, and M. Tripathy, "Performance of building integrated photovoltaic thermal system with PV module installed at optimum tilt angle and influenced by shadow," *Renew. Energy*, vol. 127, pp. 11–23, Nov. 2018.
[80] I. Jamil, J. Zhao, L. Zhang, R. Jamil, and S. F. Rafique, "Evaluation of energy production and energy yield assessment based on feasibility, design, and execution of 3 × 50 MW grid-connected solar PV pilot project in Nooriabad," *Int. J. Photoenergy*, vol. 2017, pp. 1–18, Nov. 2017.
[81] A. H. A. Al-Waeli, H. A. Kazem, K. Sopian, and M. T. Chaichan, "Techno-economical assessment of grid connected PV/T using nanoparticles and water as base-fluid systems in Malaysia," *Int. J. Sustain. Energy*, vol. 37, no. 6, pp. 558–575, May 2017.
[82] S. A. Ross, R. W. Westerfield, B. D. Jordan, G. S. Roberts, J. A. Pandes, and T. A. Holloway, *Fundamentals of Corporate Finance*, 10th ed. New York, NY, USA: McGraw-Hill, 2019, pp. 304–332.
[83] R. Parrino, D. S. Kidwell, and T. W. Bates, *Fundamentals of Corporate Finance*, 2nd ed. Hoboken, NJ, USA: Wiley, 2012, pp. 306–313.
[84] D. C. Howell, *Fundamental Statistics for the Behavioral Sciences*, 8th ed. Belmont, CA, USA: Cengage Learning, 2011, pp. 90–106.
[85] J. D. Brown, *Advanced Statistics for the Behavioral Sciences, A Computational Approach With R*. Cham, Switzerland: Springer, 2018, pp. 163–177.
[86] R. Darussalam, A. Rajani, and T. D. Atmaja, "Adjustment of azimuth direction and angle of photovoltaic panel tilt for solar radiation optimization, case study: Bandung—West Java," in *Proc. Phys. Nat. Seminar (SNF)*, vol. 5, Jakarta, Indonesia, Oct. 2016, pp. 31–36.
[87] A. M. Omar, M. Z. Hussin, S. Shaari, and K. Sopian, "Energy yield calculation of the grid-connected photovoltaic power system," in *Proc. 8th Int. Conf. Renew. Energy Sources (RES)*, Kuala Lumpur, Malaysia, Apr. 2014, pp. 162–167.
[88] C. Tredoux and K. Durrheim, *Numbers, Hypotheses & Conclusions; A course in Statistics for the Social Sciences*. Lansdowne, Cape Town: UCT Press, 2002, pp. 183–184.

WALUYO (Member, IEEE) was born in Magelang, Indonesia, in 1969. He received the master's and Ph.D. degrees in high voltage engineering from the Institut Teknologi Bandung (ITB), Bandung, Indonesia, in 2002 and 2010, respectively. He is currently an Associate Professor with the Department of Electrical Engineering, Institut Teknologi Nasional Bandung. His research interests include high voltage engineering and technology, power transmission, smart grid, and automation systems.

ANDRE WIDURA was born in Bandung, Indonesia, in 1979. He received the master's degree in biomedical engineering from the Institut Teknologi Bandung (ITB), in 2010. He is currently an Academic Staff with the Department of Electrical Engineering, Institut Teknologi Nasional Bandung. His research interests include biomedical engineering, solar cell, and battery.

FEBRIAN HADIATNA (Member, IEEE) was born in Bandung, Indonesia, in 1990. He received the master's degree in electronics from the Institut Teknologi Bandung (ITB), in 2016. He is currently an Academic Staff Member with the Department of Electrical Engineering, Institut Teknologi Nasional Bandung. His research interests include electronics and computers.

RANGGA MAULANA was born in Bandung, Indonesia, in 1996. He received the bachelor's degree in electrical engineering from the Department of Electrical Engineering, Institut Teknologi Nasional Bandung, in 2020. He is currently a staff with a private company. His research interests include solar power generation and power electrical engineering.